hep-th/0606096
May 2006

Quasi-normal Modes of Electromagnetic Perturbations of Four-Dimensional Topological Black Holes with Scalar Hair

George Koutsoumbas,[a,*] **Suphot Musiri,**[b,†] **Eleftherios Papantonopoulos**[a,♭]

and George Siopsis[c,♮]

[a]Department of Physics, National Technical University of Athens,
Zografou Campus GR 157 73, Athens, Greece
[b]Department of Physics, Srinakharinwirot University, Bangkok 10110, Thailand
[c]Department of Physics and Astronomy, The University of Tennessee, Knoxville, TN 37996 - 1200, USA

Abstract

We study the perturbative behaviour of topological black holes with scalar hair. We calculate both analytically and numerically the quasi-normal modes of the electromagnetic perturbations. In the case of small black holes we find evidence of a second-order phase transition of a topological black hole to a hairy configuration.

* kutsubas@central.ntua.gr
† suphot@swu.ac.th
♭ lpapa@central.ntua.gr
♮ siopsis@tennessee.edu

1 Introduction

Quasi-normal modes (QNMs) are well known to play an important role in black hole physics. They determine the late-time evolution of fields in the black hole exterior. After an initial perturbation the black hole starts vibrating into quasi-normal oscillation modes whose frequencies and decay times depend only on the intrinsic features of the black hole itself being insensitive to the details of the initial perturbation. For these reasons, QNMs of black holes in asymptotically flat spacetimes have been extensively studied (for reviews, see [1, 2]).

The Anti-de Sitter - conformal field theory (AdS/CFT) correspondence has led to an intensive investigation of black hole QNMs in asymptotically AdS spacetimes. Quasi-normal modes in AdS spacetime were first computed for a conformally invariant scalar field, whose asymptotic behaviour is similar to flat spacetime [3]. Subsequently, motivated by the AdS/CFT correspondence, Horowitz and Hubeny made a systematic computation of QNMs for scalar perturbations of Schwarzschild-AdS (S-AdS) spacetimes [4]. Their work was extended to gravitational and electromagnetic perturbations of S-AdS black holes in [5]. The study of scalar perturbations was further extended to the case of Reissner-Nordström-AdS (RN-AdS) black holes in [6]. Finally, the QNMs of scalar, electromagnetic and gravitational perturbations of RN-AdS black holes were presented in [7] using the results of [8].

In a parallel development, exact black hole solutions in asymptotically non-flat spacetimes were studied recently and solutions with scalar hair and negative cosmological constant were found. Exact black hole solutions are known in three [9, 10] and four dimensions [11]. For asymptotically flat spacetime, a four-dimensional black hole is also known, but the scalar field diverges at the horizon [12]. Also spherically symmetric black hole solutions have been found numerically in four [13, 14] and five dimensions [15]. Spaces with a negative cosmological constant also allow for the existence of black holes whose horizon has nontrivial topology in four [16, 17, 18, 19] and higher dimensions [20, 21, 22, 23] as well as for gravity theories containing higher powers of the curvature [24, 25, 26, 27].

Recently, an exact black hole solution in four dimensions with a minimally coupled self-interacting scalar field, in an asymptotically locally anti-de Sitter spacetime, was found [28] (MTZ black hole). The event horizon is a surface of negative constant curvature enclosing the curvature singularity at the origin. It was shown that there is a second-order phase transition at a critical temperature below which a black hole in vacuum undergoes a spontaneous dressing up with a nontrivial scalar field. An extension of the above solution including a charge was presented in [29]. Aspects of the thermodynamics of the MTZ black hole are discussed in [30]. In [31] it was shown that the four-dimensional MTZ black hole can be uplifted to eleven dimensions in supergravity theory.

In this work, we make a perturbative study of the MTZ black hole. We compute the simplest possible QNMs of the MTZ black hole, those of electromagnetic (EM) perturbations. The computation is carried out both analytically and numerically with fairly good agreement. The QNMs provide, near a critical temperature and for small black holes, support for the claim that a vacuum topological black hole (TBH) goes over to a hairy configuration, the MTZ black hole, through a second-order phase transition.

The paper is organized as follows. In section 2, we review the MTZ black hole and its charged extension. In section 3, we discuss the thermodynamics of the MTZ and TBH black holes. In section 4, we calculate the QNMs of the EM perturbations analytically whereas in Section 5 we present the numerical computation of the QNMs and compare them with the analytical results of section 4. Finally, section 6 contains our conclusions.

2 Four-Dimensional Topological Black Hole with Scalar Hair

Consider four-dimensional gravity with negative cosmological constant ($\Lambda = -3l^{-2}$) and a scalar field described by the action

$$I = \int d^4x\sqrt{-g}\left[\frac{R+6l^{-2}}{16\pi G} - \frac{1}{2}g^{\mu\nu}\partial_\mu\phi\partial_\nu\phi - V(\phi)\right] , \tag{2.1}$$

where l is the AdS radius, and G is the Newton's constant. The self-interaction potential is given by

$$V(\phi) = -\frac{3}{4\pi G l^2}\sinh^2\sqrt{\frac{4\pi G}{3}}\phi , \tag{2.2}$$

which has a global maximum at $\phi = 0$, and has a mass term given by $m^2 = V''|_{\phi=0} = -2l^{-2}$. This mass satisfies the Breitenlohner-Friedman bound that ensures the perturbative stability of AdS spacetime [32, 33]. The field equations are

$$\begin{aligned} G_{\mu\nu} - \frac{3}{l^2}g_{\mu\nu} &= 8\pi G\, T_{\mu\nu} , \\ \Box\phi - \frac{dV}{d\phi} &= 0 , \end{aligned} \tag{2.3}$$

where $\Box \equiv g^{\mu\nu}\nabla_\mu\nabla_\nu$, and the stress-energy tensor is given by

$$T_{\mu\nu} = \partial_\mu\phi\partial_\nu\phi - \frac{1}{2}g_{\mu\nu}g^{\alpha\beta}\partial_\alpha\phi\partial_\beta\phi - g_{\mu\nu}V(\phi) . \tag{2.4}$$

A static black hole solution with topology $\mathbb{R}^2 \times \Sigma$, where Σ is a two-dimensional manifold of negative constant curvature, is given by [28]

$$ds^2 = \frac{r(r+2G\mu)}{(r+G\mu)^2}\left[-\left(\frac{r^2}{l^2} - \left(1+\frac{G\mu}{r}\right)^2\right)dt^2 + \left(\frac{r^2}{l^2} - \left(1+\frac{G\mu}{r}\right)^2\right)^{-1}dr^2 + r^2 d\sigma^2\right] , \tag{2.5}$$

and the scalar field is

$$\phi = \sqrt{\frac{3}{4\pi G}}\,\mathrm{Arctanh}\frac{G\mu}{r+G\mu} . \tag{2.6}$$

The position of the horizon is at r_+, which is the solution of

$$G\mu = \frac{r_+^2}{l} - r_+ . \tag{2.7}$$

For $\phi = 0$ we get the vacuum solution (Topological Black Hole (TBH)) [16, 17, 18, 19]

$$ds_0^2 = -\left[\frac{r^2}{l^2} - 1 - \frac{2G\mu}{r}\right] dt^2 + \left[\frac{r^2}{l^2} - 1 - \frac{2G\mu}{r}\right]^{-1} dr^2 + r^2 d\sigma^2 \ . \tag{2.8}$$

A charged black hole with scalar hair was presented in [29]. The action is given by

$$\begin{aligned} I &= \int d^4x\sqrt{-g}\left[\frac{R+6l^{-2}}{16\pi G} - \frac{1}{2}g^{\mu\nu}\partial_\mu\phi\partial_\nu\phi - \frac{1}{12}R\phi^2 - \alpha\phi^4\right] \\ &\quad -\frac{1}{16\pi}\int d^4x\sqrt{-g}F^{\mu\nu}F_{\mu\nu} \ , \end{aligned} \tag{2.9}$$

where α is an arbitrary coupling constant.

The corresponding field equations are

$$\begin{aligned} G_{\mu\nu} - \frac{3}{l^2}g_{\mu\nu} &= 8\pi G(T^\phi_{\mu\nu} + T^{\rm em}_{\mu\nu}) \ , \\ \Box\phi &= \frac{1}{6}R\phi + \alpha\phi^3 \ , \\ \partial_\nu(\sqrt{-g}F^{\mu\nu}) &= 0 \ , \end{aligned} \tag{2.10}$$

and the energy-momentum tensor is given by the sum of

$$T^\phi_{\mu\nu} = \partial_\mu\phi\partial_\nu\phi - \frac{1}{2}g_{\mu\nu}g^{\alpha\beta}\partial_\alpha\phi\partial_\beta\phi + \frac{1}{6}[g_{\mu\nu}\Box - \nabla_\mu\nabla_\nu + G_{\mu\nu}]\phi^2 - g_{\mu\nu}\alpha\phi^4, \tag{2.11}$$

and

$$T^{\rm em}_{\mu\nu} = \frac{1}{4\pi}\left(F_{\mu\alpha}F_{\nu\beta} - \frac{1}{4}g_{\mu\nu}F_{\gamma\alpha}F_{\delta\beta}g^{\gamma\delta}\right)g^{\alpha\beta}. \tag{2.12}$$

The charged static black hole solution with topology $\mathbb{R}^2 \times \Sigma$ is given by

$$ds^2 = -\Big[\frac{r^2}{l^2} - \Big(1 + \frac{G\mu}{r}\Big)^2\Big]dt^2 + \Big[\frac{r^2}{l^2} - \Big(1 + \frac{G\mu}{r}\Big)^2\Big]^{-1}dr^2 + r^2 d\sigma^2, \tag{2.13}$$

where $-\infty < t < \infty$ and $r > 0$. The scalar field is

$$\phi = \sqrt{\frac{1}{2\alpha l^2}}\frac{G\mu}{(r + G\mu)} \ , \tag{2.14}$$

with $\alpha > 0$ and the only non-zero component of the electromagnetic field is

$$A_t = -\frac{q}{r} \ . \tag{2.15}$$

The integration constants q and μ are not independent. They are related by

$$q^2 = -G\mu^2\left(1 - \frac{2\pi G}{3\alpha l^2}\right) \ . \tag{2.16}$$

They correspond to conserved charges,

$$M = \frac{\sigma}{4\pi}\mu \quad \text{and} \quad Q = \frac{\sigma}{4\pi}q \ , \tag{2.17}$$

respectively, where σ denotes the area of Σ.

Eq. (2.16) fixes a charge-to-mass ratio for this black hole, which is a function of the constants appearing in the action, G and α. Moreover, eq. (2.16) determines an upper bound for α

$$0 < \alpha \leq \frac{2\pi G}{3l^2} \ . \tag{2.18}$$

If the upper bound is saturated, the charge vanishes. Then we recover the MTZ black hole. Indeed the form of the self-interacting potential considered in (2.2) can be naturally obtained through the relation between the conformal and Einstein frames [28].

Note that if $\mu = 0$ then both the MTZ black hole (2.5) and the TBH black hole (2.8) go to

$$ds^2_{AdS} = -\left[\frac{r^2}{l^2} - 1\right] dt^2 + \left[\frac{r^2}{l^2} - 1\right]^{-1} dr^2 + r^2 d\sigma^2 \ , \tag{2.19}$$

which is a manifold of negative constant curvature possessing an event horizon at $r = l$. We can say that as $\phi \to 0$ the MTZ and TBH black holes match continuously at $\mu = 0$ or $r = l$ with (2.19) being a transient configuration as it becomes apparent in the following. In the sequel we set $l = 1$.

3 Thermodynamics

For the MTZ black hole, the temperature, entropy and mass are given respectively by [28]

$$\begin{aligned} T &= \frac{2r_+ - 1}{2\pi} \ , \\ S &= \frac{\sigma r_+(r_+ + 2G\mu)}{4G(r_+ + G\mu)^2} r_+^2 = \frac{\sigma}{4G}(2r_+ - 1) \ , \\ M &= \frac{\sigma\mu}{4\pi} = \frac{\sigma(r_+^2 - r_+)}{4\pi G} \ . \end{aligned} \tag{3.1}$$

Notice that the entropy in this case does not satisfy an area law. It is easy to show that the law of thermodynamics $dM = TdS$ holds. Defining the free energy as $F = M - TS$ and using relations (3.1), we obtain

$$F_{MTZ} = -\frac{\sigma}{8\pi G}(2r_+^2 - 2r_+ + 1) \ . \tag{3.2}$$

The free energy (3.2) can be written as

$$F_{MTZ} = -\frac{\sigma}{8\pi G}\Big(1 + 2(T - T_0)\pi + 2(T - T_0)^2\pi^2\Big) \ , \tag{3.3}$$

where $T_0 = 1/2\pi \approx 0.160$ is the critical temperature. For the vacuum TBH black hole (denoting by ρ_+ the horizon for this case) , the temperature, entropy and mass are, respectively,

$$\begin{aligned} T &= \frac{3\rho_+^2 - 1}{4\pi\rho_+} \ , \\ S &= \frac{\sigma\rho_+^2}{4G} \ , \\ M &= \frac{\sigma(\rho_+^3 - \rho_+)}{8\pi G} \ . \end{aligned} \tag{3.4}$$

Then, the free energy of the TBH black hole, using relations (3.4), is

$$F_{TBH} = -\frac{\sigma}{16\pi G}(\rho_+^3 + \rho_+) \ , \tag{3.5}$$

which can be expanded around the critical temperature T_0 as

$$F_{TBH} = -\frac{\sigma}{8\pi G}\Big(1 + 2(T - T_0)\pi + 2(T - T_0)^2\pi^2 + (T - T_0)^3\pi^3 + \dots\Big) \ . \tag{3.6}$$

Using (3.3) and (3.6), we can calculate the difference between the TBH and MTZ free energies. We obtain

$$\Delta F = F_{TBH} - F_{MTZ} = -\frac{\sigma}{8\pi G}(T - T_0)^3\pi^3 + \dots \ , \tag{3.7}$$

indicating a phase transition between MTZ and TBH at the critical temperature T_0. Matching the temperatures of the MTZ black hole and the TBH we get:

$$T = \frac{2r_+ - 1}{2\pi} = \frac{1}{4\pi}\left(3\rho_+ - \frac{1}{\rho_+}\right) \Rightarrow r_+ = \frac{3\rho_+}{4} - \frac{1}{4\rho_+} + \frac{1}{2} \ . \tag{3.8}$$

It is easily seen that $r_+ \leq \rho_+$, and the inequality is saturated for $r_+ = \rho_+ = 1$. We remark that the temperature T should be non-negative, so $r_+ \geq \frac{1}{2}$ for the MTZ black hole and $\rho_+ \geq \frac{1}{\sqrt{3}}$ for the TBH black hole.

Thermodynamically we can understand this phase transition as follows. Using relations (3.1), (3.4) and (3.8), we find that $S_{TBH} > S_{MTZ}$ and $M_{TBH} > M_{MTZ}$ for the relevant ranges of the horizons r_+ or ρ_+. If $r_+ > 1$ $(T > T_0)$, both black holes have positive mass. As $T > T_0$ implies $F_{TBH} \leq F_{MTZ}$, the MTZ black hole dressed with the scalar field will decay into the bare black hole. In the decay process, the scalar black hole absorbs energy from the thermal bath, increasing its horizon radius (from r_+ to $\rho_+ > r_+$) and consequently its entropy. Therefore, in a sense the scalar field is absorbed by the black hole.

If $r_+ < 1$ $(T < T_0)$, both black holes have negative mass, but now $F_{TBH} > F_{MTZ}$, which means that the MTZ configuration with nonzero scalar field is favorable. As a consequence, below the critical temperature, the bare black hole undergoes a spontaneous "dressing up" with the scalar field. In the process, the mass and entropy of the black hole decrease and the differences in energy and entropy are transferred to the heat bath.

At the critical temperature, the thermodynamic functions of the two phases match continuously, hence, the phase transition is of second order. The order parameter that characterizes the transition can be defined in terms of the value of the scalar field at the horizon; using the solution for the scalar field (2.6) we obtain for $T < T_0$,

$$\lambda_\phi = \left| \tanh \sqrt{\frac{4\pi G}{3}} \phi(r_+) \right| = \left| \frac{r_+ - 1}{r_+} \right| = \frac{T_0 - T}{T_0 + T} \quad . \tag{3.9}$$

For $T > T_0$, λ_ϕ vanishes. Then the relation (3.7) can be written in terms of the order parameter λ_ϕ as

$$\Delta F = F_{TBH} - F_{MTZ} = +\frac{\sigma r_+^3}{8\pi G} \lambda_\phi^3 + \dots \qquad (T < T_0). \tag{3.10}$$

The pure AdS space of (2.19) has free energy $F_{AdS} = -\sigma/8\pi G$ as easily can be seen using relations (3.2) or (3.5) with $r_+ = 1$. Then observe that F_{AdS} is the constant term of both F_{MTZ} in (3.3) and F_{TBH} in (3.6). Hence the difference of free energies of MTZ or TBH black holes with the free energy of pure AdS space indicates that the configuration (2.19) is transient between the MTZ and TBH phase transition.

In the next two sections we will find the QNMs of the electromagnetic perturbations of the MTZ black hole and its charged generalization and compare them with the corresponding QNMs of the TBH. This study will provide additional information on the stability of the MTZ black hole and its generalization under electromagnetic perturbations. Note that for the MTZ black hole and its charged generalization, the wave equations, after factoring out the angular parts, are the same. For the TBH, only the function $f(r)$ (eq. (4.2)) changes. There is no change due to the axial or polar character of the perturbation.

4 Analytical Calculation

In this section, we calculate analytically the QNMs of electromagnetic perturbations for both MTZ and topological black holes. Numerical results will be discussed in section 5. Our approach is based on the method discussed in [34, 35, 36]. In order to calculate QNMs, in general, one solves the wave equation subject to appropriate boundary conditions at infinity and the horizon. In asymptotically flat spacetime, this can be implemented by a monodromy method [37]. It is then advantageous to follow Stokes lines which go through the black hole singularity. In asymptotically (A)dS spacetimes, the calculation simplifies because the wavefunction vanishes at infinity. Although the monodromy does not enter the calculation, in several cases it is still advantageous to follow Stokes lines and analytically continue the wavefunction through the black hole singularity [34, 35, 36]. However, this is not always necessary, if a general solution (or approximation thereof) of the wave equation as in, e.g., [38] is readily available. In our case, we shall solve the wave equation near the black hole singularity perturbatively and then analytically continue the wavefunction in order to match with the expected behaviour at infinity and the horizon, respectively. This will produce an explicit form of the QNMs for $r_+ > 1$ ($G\mu > 0$). For $r_+ < 1$ ($G\mu < 0$), we

do not have explicit analytical expressions. Instead, we obtain a lower bound which is in accord with numerical results.

Electromagnetic perturbations obey the wave equation

$$f(r)\frac{d}{dr}\left(f(r)\frac{d\Psi_\omega}{dr}\right)+\left[\omega^2-\left(\xi^2+\frac{1}{4}\right)\frac{f(r)}{r^2}\right]\Psi_\omega=0\ , \tag{4.1}$$

where

$$f_{MTZ}(r)=r^2-\left(1+\frac{G\mu}{r}\right)^2\quad ,\qquad f_{TBH}(r)=r^2-1-\frac{2G\mu}{r}\ . \tag{4.2}$$

It may be cast into a Schrödinger-like form if written in terms of the tortoise coordinate defined by

$$\frac{dx}{dr}=\frac{1}{f(r)}\ . \tag{4.3}$$

We obtain

$$-\frac{d^2\Psi_\omega}{dx^2}+V(x)\Psi_\omega=\omega^2\Psi_\omega\ , \tag{4.4}$$

where the potential is

$$V[x(r)]=\left(\xi^2+\frac{1}{4}\right)\frac{f(r)}{r^2}\ . \tag{4.5}$$

For QNMs, we impose the boundary condition $\Psi_\omega\to 0$ as $r\to\infty$, since the potential does not vanish for large r. At the horizon ($x\to-\infty$), we demand $\Psi_\omega\sim e^{i\omega x}$ (ingoing wave).

Near the black hole singularity ($r\sim 0$), the tortoise coordinate (4.3) may be approximated by

$$x\approx-\frac{G\mu}{a\lambda}\left(\frac{r}{G\mu}\right)^\lambda\ , \tag{4.6}$$

where $a=1$, $\lambda=3$ for MTZ and $a=2$, $\lambda=2$ for TBH. In arriving at (4.6), we choose the integration constant so that $x=0$ at $r=0$. The potential near the singularity is

$$V(x)\approx-\frac{\mathcal{A}}{x^{1+1/\lambda}}\quad ,\qquad \mathcal{A}=\left(\xi^2+\frac{1}{4}\right)\frac{1}{(aG\mu)^{1-1/\lambda}(-\lambda)^{1+1/\lambda}}\ . \tag{4.7}$$

We will solve the wave eq. (4.4) by treating the potential (4.7) as a perturbation. The zeroth-order solutions are

$$\Psi_0^\pm=e^{\pm i\omega x} \tag{4.8}$$

and the first-order corrections are

$$\Psi_1^\pm(x)=\frac{1}{2i\omega}\int_0^x dx' e^{i(\omega-i\epsilon)(x-x')}V(x')\Psi_0^\pm(x')-\frac{1}{2i\omega}\int_0^x dx' e^{-i(\omega+i\epsilon)(x-x')}V(x')\Psi_0^\pm(x') \tag{4.9}$$

where we included a small $\epsilon>0$ to render integrals finite. We shall work with general values of λ in the potential (4.7) and take the limit of interest ($\lambda\to 2,3$) at the end of the calculation. The desired solution will be a linear combination of the above wave functions,

$$\Psi_\omega(x)=A_+(\Psi_0^+ +\Psi_1^+)+A_-(\Psi_0^- +\Psi_1^-)\ . \tag{4.10}$$

Asymptotically, it behaves as

$$\Psi_\omega(x) \approx \left(A_+ + ie^{\frac{i\pi}{2\lambda}}\frac{\mathcal{A}\Gamma(-1/\lambda)}{(2\omega)^{1-1/\lambda}}A_-\right)e^{i\omega x} + \left(A_- - ie^{-\frac{i\pi}{2\lambda}}\frac{\mathcal{A}\Gamma(-1/\lambda)}{(2\omega)^{1-1/\lambda}}A_+\right)e^{-i\omega x} \ . \quad (4.11)$$

At large r ($x \to +\infty$), the tortoise coordinate (4.3) may be approximated by

$$x \approx x_0 - \frac{1}{r} \ , \quad x_0 = \int_0^\infty \frac{dr}{f(r)} \quad (4.12)$$

and the potential (4.7) is

$$V(x) \approx \xi^2 + \frac{1}{4} \ . \quad (4.13)$$

Since we are interested in the asymptotic form of quasi-normal frequencies, we may ignore the potential ($V(x) \lesssim \omega^2$). We obtain the eigenfunction for large r ($x \sim x_0$)

$$\Psi_\omega(x) \sim \sin\omega(x - x_0) \ , \quad (4.14)$$

where we applied the boundary condition $\Psi_\omega \to 0$ as $r \to \infty$ ($x \to x_0$).

This is matched by the linear combination (4.11) provided

$$A_+ + ie^{\frac{i\pi}{2\lambda}}\frac{\mathcal{A}\Gamma(-1/\lambda)}{(2\omega)^{1-1/\lambda}}A_- = -e^{-2i\omega x_0}\left(A_- - ie^{-\frac{i\pi}{2\lambda}}\frac{\mathcal{A}\Gamma(-1/\lambda)}{(2\omega)^{1-1/\lambda}}A_+\right) \quad (4.15)$$

of eigenfunction (eqs. (4.8) and (4.9)) in the vicinity of the singularity.

Next, we approach the horizon ($x \to -\infty$) by analytically continuing (4.10) to negative x. This amounts to a rotation by $-\pi$ in the complex x-plane. For $x < 0$, we obtain from (4.9), using eqs. (4.7) and (4.8),

$$\Psi_1^\pm(x) = \frac{\mathcal{A}}{2i\omega}e^{i\pi/\lambda}\int_0^{-x}\frac{dx'}{{x'}^{1+1/\lambda}}\left(e^{i(\omega+i\epsilon)(x+x')} - e^{-i(\omega-i\epsilon)(x+x')}\right)e^{\mp i\omega x'}. \quad (4.16)$$

Taking the limit $x \to -\infty$, we obtain the behavior near the horizon

$$\Psi_\omega(x) \approx \left(A_+ - ie^{\frac{3i\pi}{2\lambda}}\frac{\mathcal{A}\Gamma(-1/\lambda)}{(2\omega)^{1-1/\lambda}}A_-\right)e^{i\omega x} + \left(A_- + ie^{\frac{i\pi}{2\lambda}}\frac{\mathcal{A}\Gamma(-1/\lambda)}{(2\omega)^{1-1/\lambda}}A_+\right)e^{-i\omega x} \ . \quad (4.17)$$

Since we want an ingoing wave ($\Psi_\omega \sim e^{i\omega x}$) at the horizon, we obtain the constraint on the coefficients

$$A_- + ie^{\frac{i\pi}{2\lambda}}\frac{\mathcal{A}\Gamma(-1/\lambda)}{(2\omega)^{1-1/\lambda}}A_+ = 0 \ . \quad (4.18)$$

For compatibility with the other constraint (4.15), we ought to have

$$\begin{vmatrix} e^{-2i\omega x_0} + e^{\frac{i\pi}{2\lambda}}\mathcal{C} & 1 \\ 1 - \mathcal{C}e^{-\frac{i\pi}{2\lambda}}e^{-2i\omega x_0} & \mathcal{C}e^{-\frac{i\pi}{2\lambda}} \end{vmatrix} = 0 \ , \quad (4.19)$$

where $\mathcal{C} = i\mathcal{A}\Gamma(-1/\lambda)(2\omega)^{-1+1/\lambda}$. We deduce

$$e^{2i\omega x_0} = 2e^{-\frac{i\pi}{2\lambda}}\mathcal{C} \ , \quad (4.20)$$

where we discarded terms which were of order higher than linear in $\mathcal{C}$. Solving for ω, we obtain the quasi-normal frequencies

$$\omega_n = \frac{n\pi}{x_0} + o(\ln n) \ . \tag{4.21}$$

Thus the asymptotic behaviour is completely determined by the parameter x_0 (eq.(4.12)).

In the case of MTZ black holes, $f(r)$ has four roots,

$$r_\pm = \frac{1}{2}\left(1 \pm \sqrt{1+4G\mu}\right) \quad , \quad \bar{r}_\pm = \frac{1}{2}\left(-1 \pm \sqrt{1-4G\mu}\right) \ . \tag{4.22}$$

For $G\mu > 0$, the horizon is at r_+ and $r_+ > 1$. We obtain

$$x_0 = \frac{1}{2(r_+ - r_-)} \ln \frac{r_-}{r_+} + \frac{1}{2(\bar{r}_+ - \bar{r}_-)} \ln \frac{\bar{r}_-}{\bar{r}_+} \ . \tag{4.23}$$

For large $G\mu$, the quasi-normal frequencies are

$$\omega_n \approx 2(1-i) r_+ n \tag{4.24}$$

matching the behaviour in *five*-dimensional AdS space.

For small (positive) $G\mu$, we find

$$\omega_n \approx -2ni\left(1 + \frac{2G\mu}{\pi i} \ln G\mu\right) \ . \tag{4.25}$$

Continuing to negative values of $G\mu$ is not straightforward. The above discussion is not applicable, because going beyond the horizon (as we approach the singularity) we encounter a potential well at $r_- < r < r_+$ for $G\mu > -1/4$ (horizon $1/2 < r_+ < 1$) which admits bound states and alters the behaviour of quasi-normal frequencies. The minimum of the potential provides a lower bound to the frequencies. By setting $V'(r) = 0$, we find the minimum at

$$r_{min} = -2G\mu \ . \tag{4.26}$$

At the minimum,

$$V(r_{min}) = -\left(\xi^2 + \frac{1}{4}\right)\left\{\frac{1}{16(G\mu)^2} - 1\right\} \ . \tag{4.27}$$

It is also easily seen that $V''(r_{min}) > 0$, showing that $r = r_{min}$ is indeed a minimum. The eigenfrequencies have imaginary part

$$\omega_I \geq -\sqrt{|V(r_{min})|} \ , \tag{4.28}$$

which is verified by numerical results. The lowest frequency is close to the lower bound (4.28).

In the TBH case, the horizon is given by

$$r_+ = 2\Re(e^{i\pi/6} s) \quad , \quad s = \left(\sqrt{\frac{1}{27} - (G\mu)^2} - iG\mu\right)^{1/3} \ , \tag{4.29}$$

where $|G\mu| < 3^{-3/2}$. The other two roots of $f(r)$ are also real,

$$r_- = -2\Re(e^{-i\pi/6}s) \quad , \quad r'_- = 2\Im s \ . \tag{4.30}$$

We obtain

$$x_0 = -\frac{r_-}{3r_-^2-1}\ln\frac{r_-}{r_+} - \frac{r'_-}{3r'^2_--1}\ln\frac{r'_-}{r_+} \ . \tag{4.31}$$

For small $G\mu$, we have

$$\omega_n \approx -2ni\left(1+\frac{4G\mu}{\pi i}\ln G\mu\right) \tag{4.32}$$

to be compared with the behaviour of MTZ QNMs (4.25) near the transition point. The discrepancy is of second order.

For large $G\mu$, the above formulae for the roots read

$$r_+ = \left(G\mu+\sqrt{(G\mu)^2-\frac{1}{27}}\right)^{1/3} + \left(G\mu-\sqrt{(G\mu)^2-\frac{1}{27}}\right)^{1/3} \approx (2G\mu)^{1/3} \ ,$$

$$r_- = -e^{-\frac{i\pi}{3}}\left(G\mu+\sqrt{(G\mu)^2-\frac{1}{27}}\right)^{1/3} - e^{+\frac{i\pi}{3}}\left(G\mu-\sqrt{(G\mu)^2-\frac{1}{27}}\right)^{1/3} \approx -e^{-\frac{i\pi}{3}}r_+ \ ,$$

$$r'_- = (r_-)^* \approx -e^{+\frac{i\pi}{3}}r_+ \ . \tag{4.33}$$

Then

$$\omega_n \approx nr_+\left(\frac{3\sqrt{3}}{4}-i\frac{9}{4}\right). \tag{4.34}$$

For $G\mu < 0$, we encounter a potential well behind the horizon. Arguing as in the MTZ case, we obtain a lower bound

$$\omega_I \geq -\sqrt{|V(r_{min})|} \tag{4.35}$$

In the TBH case, $r_{min} = -3G\mu$ and

$$V(r_{min}) = -\left(\xi^2+\frac{1}{4}\right)\left\{\frac{1}{27(G\mu)^2}-1\right\} \tag{4.36}$$

5 Numerical Results

5.1 The Method

Another method of studying the same problem is the procedure of Horowitz and Hubeny [4]. We briefly review the method as we applied it to our problem. After performing the transformation $\Psi_\omega(r) = \psi_\omega(r)e^{-i\omega r_*}$, the wave equation (4.1) becomes

$$f(r)\frac{d^2\psi_\omega(r)}{dr^2} + \left(\frac{df(r)}{dr}-2i\omega\right)\frac{d\psi_\omega(r)}{dr} = \frac{\left(\xi^2+\frac{1}{4}\right)}{r^2}\psi_\omega(r) \ . \tag{5.1}$$

The change of variables $r = 1/x$ (not to be confused with the tortoise coordinate (4.3)) yields an equation of the form

$$s(x)\left[(x-x_+)^2\frac{d^2\psi_\omega(x)}{dx^2}\right] + t(x)\left[(x-x_+)\frac{d\psi_\omega(x)}{dx}\right] + u(x)\psi_\omega(x) = 0 \ ,$$

where $x_+ = 1/r_+$. It turns out that $s(x), t(x)$ and $u(x)$ are polynomials of third degree for MTZ black holes and of second degree for TBHs. Thus,

$$\begin{aligned} s(x) &= s_0 + s_1(x-x_+) + s_2(x-x_+)^2 + s_3(x-x_+)^3, \\ t(x) &= t_0 + t_1(x-x_+) + t_2(x-x_+)^2 + t_3(x-x_+)^3, \\ u(x) &= u_0 + u_1(x-x_+) + u_2(x-x_+)^2 + u_3(x-x_+)^3 \ . \end{aligned}$$

Expanding the wavefunction around the (inverse) horizon x_+,

$$\psi_\omega(x) = \sum_0^\infty a_n(\omega)(x-x_+)^n \ , \tag{5.2}$$

we arrive at a recurrence formula for the coefficients,

$$a_n(\omega) = -\frac{1}{n(n-1)s_0 + nt_0 + u_0}\sum_{m=n-3}^{n-1}[m(m-1)s_{n-m} + mt_{n-m} + u_{n-m}]a_m(\omega) \ . \tag{5.3}$$

We note that the few coefficients $a_m(\omega)$ with negative index m which will appear for $n < 2$ should be set to zero, while $a_0(\omega)$ is set to one. Since the wave function should vanish at infinity ($r \to \infty, x = 0$), we deduce

$$\psi_\omega(0) \equiv \sum_0^\infty a_n(\omega)(-x_+)^n = 0 \ . \tag{5.4}$$

The solutions of this equation are precisely the quasi-normal frequencies.

5.2 MTZ Black Holes

We compute the QNMs for the MTZ black holes by solving eq. (5.4) numerically. As a first step we draw the contours $\Re[\psi_\omega(0)] = 0$ and $\Im[\psi_\omega(0)] = 0$ on the complex $\omega-$plane and check the points of intersection. This provides good initial values for the subsequent Müller root-finding technique [39]; in addition it provides an overview of the (approximate) values of the quasi-normal frequencies. In Fig. 1 we show sample contours for the case $r_+ = 5.0,\ \xi = 1.0$. We note that the parameter ξ does not seem to play a significant role in the behaviour of quasi-normal frequencies, so we set it to a typical value ($\xi = 1.0$) from now on.

From Fig. 1, it is evident that the QNMs lie on a straight line with *negative* slope and their spacing is more or less constant. In fact the spacing changes a little as we move to the right and eventually attains an asymptotic value, which should be compared with the analytical results of section 4.

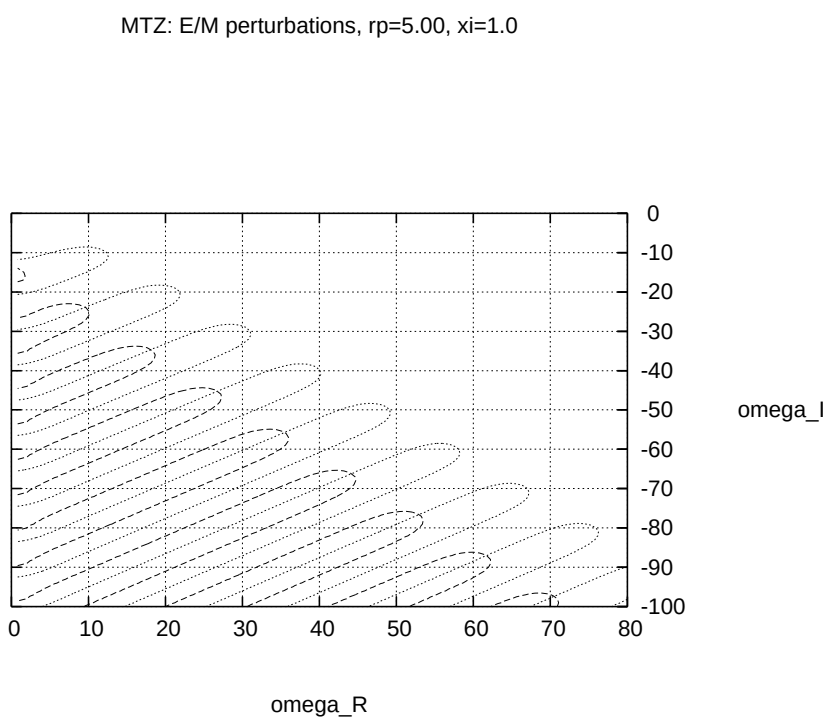

Figure 1: Contours displaying the lines $\Re[\psi_0(\omega)] = 0$ (dashed lines) and $\Im[\psi_0(\omega)] = 0$ (dotted lines) on the complex $\omega-$plane for MTZ Black Holes and $r_+ = 5.0$.

Fig. 2 refers to $r_+ = 0.97$, a typical value of the horizon radius smaller than the critical value $r_+ = 1.0$. The striking feature of the QNMs here is that the slope is *positive.* In addition, the intersections no longer lie along a straight line and the spacing changes substantially as we move through the QNMs.

To compare with analytical results, we note that equations (4.21) and (4.23) yield the asymptotic expression for QNMs. We may check that the relative sign of $\Delta\omega_R$ and $\Delta\omega_I$ is negative, therefore a larger ω_R will correspond to an algebraically smaller ω_I, as shown in Fig. 1.

For small mass ($r_+ \approx 1$), the analytical result (4.25) yields the asymptotic expression for the spacing of QNMs,

$$\Delta\omega_R \approx -\frac{4G\mu}{\pi} \ln G\mu, \;\; \Delta\omega_I \approx -2 \; . \tag{5.5}$$

In Table 1, we show the results for some indicative values of the horizon radius with $r_+ \geq 1.0$. We observe that the agreement between analytical and numerical results is quite good. The agreement is exact for $r_+ = 1.0$. In fact, the slope tends to minus infinity as we approach $r_+ = 1.0$. We should point out that $\omega_I < 0$, always, so there is no sign of instability.

In Table 2 we show the QNMs for $r_+ = 0.97$, as an example of horizon radius smaller than the critical value $r_+ = 1.0$, along with the differences between consecutive values

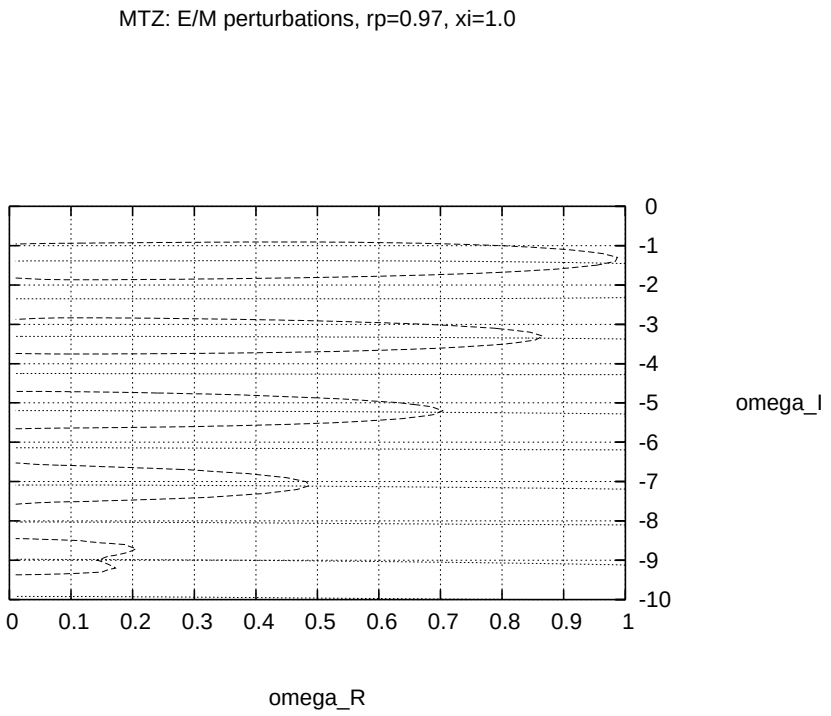

Figure 2: Contours displaying the lines $\Re[\psi_0(\omega)] = 0$ (dashed lines) and $\Im[\psi_0(\omega)] = 0$ (dotted lines) on the complex $\omega-$plane for MTZ Black Holes and $r_+ = 0.97$.

of QNMs. Note that in this case $G\mu = -0.029,\ T = 0.150$. These are the exact QNMs presented in Fig. 2. It appears that, apart from the change of the sign of the slope, there is a novel phenomenon: the quasi-normal frequencies converge toward the imaginary axis, i.e., their real part decreases. There is only a *finite* number of QNMs for $r_+ < 1.0$. This behaviour has already been predicted analytically in section 4; eq. (4.28) yields a prediction for the lowest possible imaginary part of the frequencies. The result is $\omega_I \geq -9.54i$, which is indeed respected by the imaginary parts appearing in Table 2. Although not fully justified, using the analytical result (5.5), we deduce the estimates $|\Delta\omega_R^{Ana}| \approx 0.131, \quad |\Delta\omega_I^{Ana}| \approx 2.000$. Checking against the numerical values in Table 2, we see that the values in the third column (real part) are of the same order of magnitude as the analytical prediction, whereas the values in the fourth column (imaginary part) are quite close to the analytical estimate 2. However, the variations are significant. If one further decreases the value of the horizon, the number of QNMs decreases until they finally disappear. The behavior of QNMs for such horizons may be viewed as modifications of the critical point $r_+ = 1.0$. In the latter case, the first quasi-normal frequency is $\omega = 1.0 - 1.5i$, followed by frequencies with imaginary parts $\omega_I = -3.5, -5.5, -7.5, \ldots$. Unlike the points below criticality, for $r_+ = 1.0$, the real parts do not change and there is no lower bound.

To summarize our findings, for $r_+ > 1$, Fig. 1 shows that the QNMs have a negative slope and hence large values of ω_R correspond to large values of ω_I. Then as $r_+ \to 1$ the

r_+	$G\mu$	T	$\Delta\omega_R^{Ana}$	$\Delta\omega_I^{Ana}$	$\Delta\omega_R^{Num}$	$\Delta\omega_I^{Num}$
10.000	90.00	3.023	18.96	-20.26	19.00	-20.15
5.000	20.00	1.434	8.91	-10.25	8.77	-10.45
2.000	2.000	0.477	2.75	-4.21	2.70	-4.14
1.050	0.0525	0.175	0.32	-2.15	0.27	-2.16
1.000	0.000	0.160	0.00	-2.00	0.00	-2.00

Table 1: Comparison analytical and numerical values of QNMs of EM perturbations of MTZ Black Holes.

ω_R^{Num}	ω_I^{Num}	$\Delta\omega_R^{Num}$	$\Delta\omega_I^{Num}$
0.973	-1.496	-	-
0.864	-3.351	0.109	1.905
0.701	-5.239	0.163	1.888
0.486	-7.114	0.215	1.875
0.143	-8.980	0.343	1.866

Table 2: Numerical results for quasi-normal frequencies of EM perturbations for MTZ Black Holes with $r_+ = 0.97$. In the last two columns we list the differences of consecutive QNMs.

slope tends to minus infinity. At $r_+ = 1$, $\omega_R = 1$, while the spacing of ω_I is exactly 2. Note that the critical point $r_+ = 1$ corresponds to the pure AdS configuration of (2.19). For $r_+ < 1$, Fig. 2 shows that the QNMs have a positive slope and hence large values of ω_R correspond to small values of ω_I. We attribute this behavior to a *phase transition,* as one passes through the critical value $r_+ = 1$, of the TBH to the MTZ black hole configuration.

Notice that for any perturbation of a black hole background there are two characteristic parameters that control its behaviour: the oscillation time scale which is given by $\tau_R \equiv 1/\omega_R$ and the damping time scale given by $\tau_I \equiv 1/\omega_I$. In the case of $r_+ > 1$ the scalar field is absorbed by the black hole and the damping time scale τ_I is small, so the perturbations in this case fall off rather rapidly with time. For $r_+ < 1$ the black hole is dressed up with the scalar field and the damping time scale τ_I is large and perturbations last longer. At the critical point of $r_+ = 1$ we have a change of slope, indicating a transient configuration. This behaviour may be associated with the second order phase transition discussed in section 3.

5.3 Topological Black Holes

We now turn to the case of topological black holes (TBHs). The asymptotic value of quasi-normal frequencies for $r_+ \geq 1$ is given by eqs (4.21) and (4.31). The relative sign of $\Delta\omega_R$, and $\Delta\omega_I$ is again negative.

At small masses, eq. (4.32) provides an approximate expression for QNMs in the limit of small horizon (mass) which yields the spacings

$$\Delta\omega_R \approx -\frac{8G\mu}{\pi}\ln G\mu \ , \ \Delta\omega_I \approx -2 \ . \tag{5.6}$$

The comparison of these analytical results to the numerical results of section 5 is shown in Table 3. We have used values for the horizon which correspond, through eq. (3.8), to the respective values of MTZ black holes that we showed above in Table 1 (matching corresponding temperatures). The agreement between analytical and numerical results is very good. In addition, ω_I is again negative, showing no sign of instability.

r_+	$G\mu$	T	$\Delta\omega_R^{Ana}$	$\Delta\omega_I^{Ana}$	$\Delta\omega_R^{Num}$	$\Delta\omega_I^{Num}$
12.692	1015.43	3.023	16.43	-28.55	16.50	-28.50
6.055	107.97	1.434	7.73	-13.60	7.65	-13.70
2.155	3.93	0.477	2.41	-4.78	2.52	-4.81
1.050	0.054	0.175	0.29	-2.16	0.26	-2.16
1.000	0.000	0.160	0.00	-2.00	0.00	-2.00

Table 3: Comparison of analytical and numerical values of QNMs of EM perturbations for TBHs.

Next we show the QNMs for $r_+ = 0.97$ (eq. (3.8) yields approximately the same value as in the MTZ case for the same temperature), along with differences between consecutive values of quasi-normal frequencies. Note that in this case, $G\mu = -0.029,\ T = 0.150$.

ω_R^{Num}	ω_I^{Num}	$\Delta\omega_R^{Num}$	$\Delta\omega_I^{Num}$
0.972	-1.446	-	-
0.859	-3.352	0.113	1.906
0.689	-5.240	0.170	1.888
0.453	-7.115	0.236	1.875

Table 4: Numerical results for quasi-normal frequencies of EM perturbations for TBHs with $r_+ = 0.97$. In the last two columns we list the differences of consecutive QNMs.

Similar behaviour to MTZ black holes is observed: the slope below criticality becomes *positive*, while for $r_+ > 1$ it is *negative.* Again, to compare with analytical expressions, eq. (5.6) gives the estimate $|\Delta\omega_R^{Ana}| \approx 0.259, \quad |\Delta\omega_I^{Ana}| \approx 2.000$. Checking against the entries in Table 4, we find that the values in its third and fourth columns (real and imaginary parts, respectively) are of the same order of magnitude as the analytical estimates, albeit with sizeable variations. The lower bound for the imaginary part, given by eqs. (4.28) and (4.36), reads in this case, $\omega_I \geq -7.33$, which is close to the lowest imaginary part in Table 4.

6 Conclusions

We calculated the QNMs of electromagnetic perturbations of the MTZ black hole and topological black holes. We performed this calculation both analytically and numerically with fairly good agreement. We found that there is a change in the slope of the QNMs

as we decrease the value of the horizon radius below a critical value, and we argued that this change signals a phase transition of a vacuum topological black hole toward the MTZ black hole with scalar hair.

One may attribute this change in behaviour to the dynamics of the scalar field and associate it with a second-order phase transition [28]. For small black holes ($r_+ < 1$) the scalar field is dressing up the bare topological black hole introducing an order parameter λ_ϕ (see (3.10)) which controls the dynamics of the scalar field. A second-order phase transition for small black holes occurs in more general configurations (including charge, etc) as studies of general scalar, electromagnetic and gravitational perturbations show [40]. We have also found that the vacuum AdS solution at the critical temperature is a transient configuration of the change of phase of the topological black hole to a configuration with scalar hair.

One interesting aspect of small MTZ black holes is that the quasi-normal frequencies converge toward the imaginary axis, i.e., their real part decreases and after the first few quasi-normal frequencies, it vanishes, indicating that for $r_+ < 1$ there are only a finite number of QNMs. We showed that the finite number of such modes for small horizons ($r_+ < 1$) is due to the existence of bound states behind the horizon, which is an unobservable region. This curious phenomenon is worthy of further investigation.

Acknowledgements

We thank Kostas Kokkotas for his valuable assistance in the numerical applications of this work. The work of S. M. was partially supported by the Thailand Research Fund. G. K. and E. P. were supported by (EPEAEK II)-Pythagoras (co-funded by the European Social Fund and National Resources). G. S. was supported in part by the US Department of Energy under grant DE-FG05-91ER40627.

References

[1] K. D. Kokkotas and B. G. Schmidt, Living Rev. Rel. **2**, 2 (1999) [arXiv:gr-qc/9909058].

[2] H.-P. Nollert, CQG **16**, R159-R216 (1999).

[3] J. S. F. Chan and R. B. Mann, Phys. Rev. D **55**, 7546 (1997) [arXiv:gr-qc/9612026]; Phys. Rev. D **59**, 064025 (1999).

[4] G. T. Horowitz and V. E. Hubeny, Phys. Rev. D **62**, 024027 (2000) [arXiv:hep-th/9909056].

[5] V. Cardoso and J. P. S. Lemos, Phys. Rev. D **64**, 084017 (2001) [arXiv:gr-qc/0105103].

[6] B. Wang, C. Y. Lin and E. Abdalla, Phys. Lett. B **481**, 79 (2000) [arXiv:hep-th/0003295].

[7] E. Berti and K. D. Kokkotas, Phys. Rev. D **67**, 064020 (2003) [arXiv:gr-qc/0301052].

[8] F. Mellor and I. Moss, Phys. Rev. D **41**, 403 (1990).

[9] C. Martinez and J. Zanelli, Phys. Rev. D **54**, 3830 (1996) [arXiv:gr-qc/9604021].

[10] M. Henneaux, C. Martinez, R. Troncoso and J. Zanelli, Phys. Rev. D **65**, 104007 (2002) [arXiv:hep-th/0201170].

[11] C. Martinez, R. Troncoso and J. Zanelli, Phys. Rev. D **67**, 024008 (2003) [arXiv:hep-th/0205319].

[12] N. Bocharova, K. Bronnikov and V. Melnikov, Vestn. Mosk. Univ. Fiz. Astron. **6**, 706 (1970); J. D. Bekenstein, Annals Phys. **82**, 535 (1974); Annals Phys. **91**, 75 (1975).

[13] T. Torii, K. Maeda and M. Narita, Phys. Rev. D **64**, 044007 (2001).

[14] E. Winstanley, Found. Phys. **33**, 111 (2003) [arXiv:gr-qc/0205092].

[15] T. Hertog and K. Maeda, JHEP **0407**, 051 (2004) [arXiv:hep-th/0404261].

[16] J. P. S. Lemos, Phys. Lett. B **353**, 46 (1995) [arXiv:gr-qc/9404041].

[17] R. B. Mann, Class. Quant. Grav. **14**, L109 (1997) [arXiv:gr-qc/9607071]; R. B. Mann, Nucl. Phys. B **516**, 357 (1998) [arXiv:hep-th/9705223].

[18] L. Vanzo, Phys. Rev. D **56**, 6475 (1997) [arXiv:gr-qc/9705004].

[19] D. R. Brill, J. Louko and P. Peldan, Phys. Rev. D **56**, 3600 (1997) [arXiv:gr-qc/9705012].

[20] D. Birmingham, Class. Quant. Grav. **16**, 1197 (1999) [arXiv:hep-th/9808032].

[21] R. G. Cai and K. S. Soh, Phys. Rev. D **59**, 044013 (1999) [arXiv:gr-qc/9808067].

[22] B. Wang, E. Abdalla and R. B. Mann, [arXiv:hep-th/0107243].

[23] R. B. Mann, [arXiv:gr-qc/9709039].

[24] J. Crisostomo, R. Troncoso and J. Zanelli, Phys. Rev. D **62**, 084013 (2000) [arXiv:hep-th/0003271].

[25] R. Aros, R. Troncoso and J. Zanelli, Phys. Rev. D **63**, 084015 (2001) [arXiv:hep-th/0011097].

[26] R. G. Cai, Y. S. Myung and Y. Z. Zhang, Phys. Rev. D **65**, 084019 (2002) [arXiv:hep-th/0110234].

[27] M. H. Dehghani, Phys. Rev. D **70**, 064019 (2004) [arXiv:hep-th/0405206].

[28] C. Martinez, R. Troncoso and J. Zanelli, Phys. Rev. D **70**, 084035 (2004) [arXiv:hep-th/0406111].

[29] C. Martinez, J. P. Staforelli and R. Troncoso, [arXiv:hep-th/0512022]; C. Martinez and R. Troncoso, [arXiv:hep-th/0606130].

[30] E. Winstanley, Class. Quant. Grav. **22**, 2233 (2005) [arXiv:gr-qc/0501096]; E. Radu and E. Winstanley, Phys. Rev. D **72**, 024017 (2005) [arXiv:gr-qc/0503095]; A. M. Barlow, D. Doherty and E. Winstanley, Phys. Rev. D **72**, 024008 (2005) [arXiv:gr-qc/0504087].

[31] I. Papadimitriou, [arXiv:hep-th/0606038].

[32] P. Breitenlohner and D. Z. Freedman, Phys. Lett. **B115**, 197 (1982); Annals Phys. **144**, 249 (1982).

[33] L. Mezincescu and P. K. Townsend, Annals Phys. **160**, 406 (1985).

[34] V. Cardoso, J. Natario and R. Schiappa, J. Math. Phys. **45**, 4698 (2004) [arXiv:hep-th/0403132].

[35] J. Natario and R. Schiappa, Adv. Theor. Math. Phys. **8**, 1001 (2004) [arXiv:hep-th/0411267].

[36] S. Musiri, S. Ness and G. Siopsis, Phys. Rev. D **73**, 064001 (2006) [arXiv:hep-th/0511113].

[37] L. Motl and A. Neitzke, Adv. Theor. Math. Phys. **7**, 307 (2003) [arXiv:hep-th/0301173].

[38] A. J. M. Medved, D. Martin and M. Visser, Class. Quant. Grav. **21**, 2393 (2004) [arXiv:gr-qc/0310097].

[39] W.-H. Press, S. A. Teukolsky, W. T. Vetterling and B. P. Flannery in *Numerical Recipies* (Cambridge University Press, Cambridge, England, 1992).

[40] G. Koutsoumbas, S. Musiri, E. Papantonopoulos and G. Siopsis, in preparation.